Hybrid analytical modeling of saturated linear and rotary electrical machines

Hybrid Analytical Modeling of Saturated Linear and Rotary Electrical Machines: Integration of Fourier Modeling and Magnetic Equivalent Circuits

J. Bao, B.L.J. Gysen and E.A. Lomonova
Department of Electrical Engineering, Eindhoven University of Technology, 5612 AP Eindhoven, The Netherlands

This paper presents a 2D hybrid analytical modeling method for the analysis of the magneto-static field distribution with the capability of including nonlinear materials. The model combines Fourier modeling, which is accurate and fast, with meshed magnetic equivalent circuits, which have unique permeability in mesh elements and therefore, can model local saturation. To present the diverse applicability of the proposed method, it is applied to a linear machine with permanent magnet excitation and a rotary machine with current excitation. Magnetic field calculations are compared to finite element analysis (FEA) with good agreement.

***Index Terms*—Electrical machine, analytical modeling, saturation, Fourier analysis, magnetic equivalent circuit, hybrid modeling.**

I. Introduction

MODELING of the electromagnetic field distribution is of major importance in the design process of electromagnetic devices. In recent years, several advanced methods are being researched, e.g., SchwarzChristoffel (SC) method, boundary element (BE) method, Fourier modeling, etc [1]. The SC mapping provides an analysis tool that allows the transformation from polygonal boundaries to a simpler domain, circumventing difficulties encountered when solving boundary value problems on complicated geometries [2], [3]. Facing the challenge associated with mapping function evaluation, it is developed to use SC toolbox in Matlab to automate mapping numerically [2]. It is successfully applied in [4] for a switched reluctance machine (SRM) with linear materials. The BE method is derived from the Poisson or Laplace equations in integral form. The integral equation only has to be evaluated at the boundaries of the domain, so that the number of elements can be reduced significantly compared to finite element method [3]. However, the requirement of linear material property limits the application of the method for structures involving soft-magnetic material [5].

For structures with periodicity, Fourier modeling is particularly interesting, however, the limitation is the unavailability to take circumferential variations of material property (e.g. magnetic permeability) into account [1], which is a significant drawback in the case of stator/rotor slotting [6], [7]. In [7]–[11], a hybrid analytical modeling (HAM) technique that integrates Fourier modeling and meshed magnetic equivalent circuit (MEC) is discussed. This method is capable of including small geometric features with high-permeable materials. In [8]–[11], the mesh-based MEC is only connected to one side of the Fourier modeling. A promising result of the magnetic field is provided in the airgap in [8] for a linear PM structure, and cogging force/torque is precisely estimated in [9] for various electromagnetic structures. Furthermore, material nonlinearity is shortly discussed in [10], that calculates the cogging force for PM machines with different slot geometries, considering saturation in the stator. However, the derivation of MEC formulation regarding the saturation, especially the change in source terms, is not explained. In [7], bidirectional coupling on both sides of the MEC regions are applied, achieving excellent matching of flux density in the overall

Corresponding author: J. Bao (email: j.bao@tue.nl).

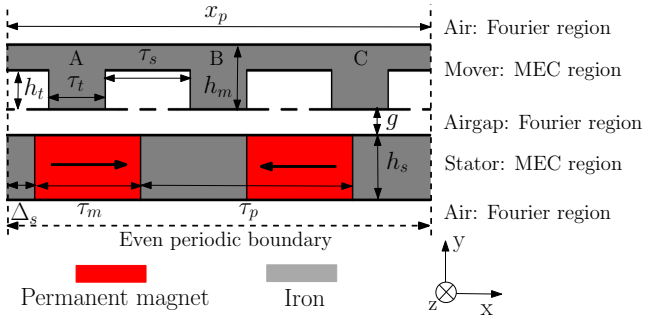

Fig. 1. Geometry of the PM machine in the Cartesian coordinate system.

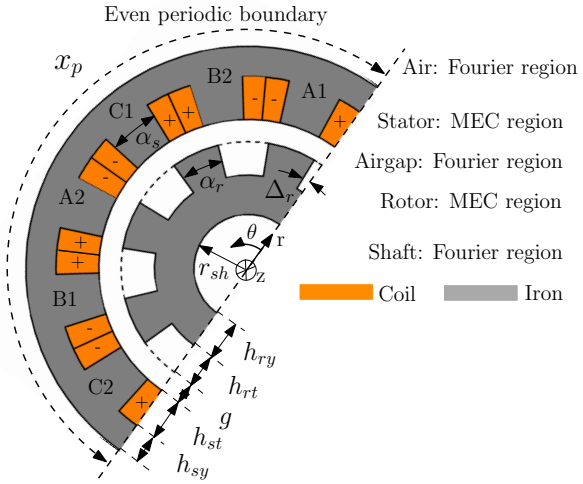

Fig. 2. Geometry of the 12/8 SRM in the polar coordinate system.

TABLE I
Dimensions of the model in Cartesian coordinate system.

Parameter	Description	value
h_m	Height of mover	5 mm
g	Airgap length	0.5 mm
h_t	Height of teeth	3 mm
h_s	Height of stator	5 mm
τ_m	Magnet width	15 mm
τ_p	Pole pitch	30 mm
Δ_s	Stator position	4 mm
τ_t	Teeth width	8 mm
τ_s	Slot width	12 mm
x_p	Width of periodicity	60 mm
L_z	Stack length	50 mm

TABLE II
Dimensions of the model in polar coordinate system.

Parameter	Description	value
r_{sh}	Shaft radius	20.5 mm
h_{ry}	Rotor yoke height	10.5 mm
h_{rt}	Rotor teeth height	14.5 mm
g	Airgap length	0.5 mm
h_{st}	Stator teeth height	14.5 mm
h_{sy}	Stator yoke height	9.5 mm
α_s	Stator tooth arc	16°
α_r	Rotor tooth arc	22°
Δ_r	Rotor position	4°
x_p	Width of periodicity	180°
L_z	Axial length	87.5 mm

TABLE III
Fourier functions in Cartesian and polar coordinate systems.

	Cartesian	polar
B_{psn}	$a_n e^{\omega_n y} + b_n e^{-\omega_n y}$	$a_n r^{\omega_n - 1} + b_n r^{-\omega_n - 1}$
B_{pcn}	$-c_n e^{\omega_n y} - d_n e^{-\omega_n y}$	$-c_n r^{\omega_n - 1} - d_n r^{-\omega_n - 1}$
B_{qsn}	$c_n e^{\omega_n y} - d_n e^{-\omega_n y}$	$c_n r^{\omega_n - 1} - d_n r^{-\omega_n - 1}$
B_{qcn}	$a_n e^{\omega_n y} - b_n e^{-\omega_n y}$	$a_n r^{\omega_n - 1} - b_n r^{-\omega_n - 1}$

Notes: spatial frequency $\omega_n = 2\pi n / x_p$.

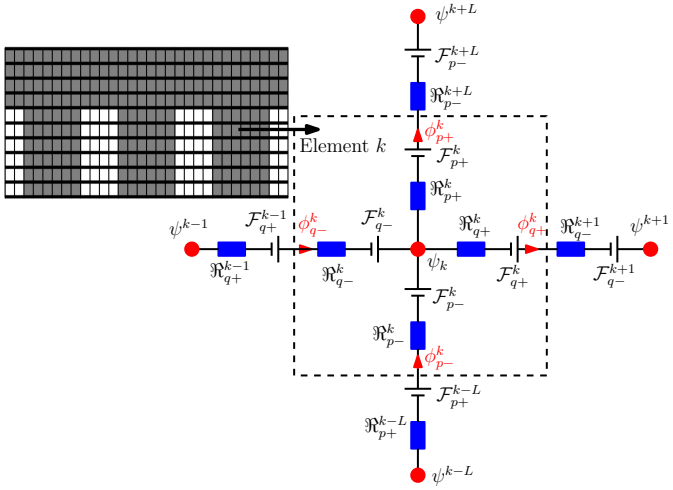

Fig. 3. Schematic graphs of a meshed MEC region and the mesh elements.

structure with linear material properties.

In this paper, the incorporation of saturation with the bidirectional-coupled HAM, is further investigated and validated by utilizing locally linearized B-H relationship for both linear and rotary machines, which are shown in Fig. 1 and Fig. 2. The content is first focused on the model formulation and description of magnetic sources (PM/current), followed by the formulation of material nonlinearity in MEC element and the iterative algorithm. Validation of the proposed method is performed by the comparison with FEA.

II. Modeling Formulation

To obtain the magnetic field solution, the following assumptions are made: 1) the problem is described in a 2D coordinate system; 2) source terms (PM/current) are invariant in the z-direction and 3) the problem is quasi static.

To present the diverse applicability of the proposed method for saturated electrical machines, it is applied to two geometries in two coordinate systems with different presences of magnetic sources (PM/current). For the Cartesian coordinate system, a slotted linear PM machine shown in Fig. 1 is modeled, and for the polar coordinate system, a three-phase 12/8 SRM [12] shown in Fig. 2 is modeled. The dimensions are given in TABLE I and TABLE II, respectively.

In the two examples, periodicities are respectively applied in the x- or θ-directions, while regions are divided in the y- or r-directions. The division in regions are shown in Fig. 1 and Fig. 2. Generally, only air and shaft regions are modeled using Fourier expressions, since Fourier modeling divides the geometry in periodical regions with homogeneous permeability and does not allow to model local saturation. The meshed MEC, on the other hand, is used for regions with nonlinear material (such as stator and mover/rotor), since each mesh element is able to have its unique permeability and hence, is capable to take local saturation into account. For generality of the explanations in the following content, the normal direction (y or r) is referred as the p-direction, while the tangential direction (x or θ) is referred as the q-direction.

A. Definition of Fourier regions

In Fourier regions, the magnetostatic problem is formulated in the terms of magnetic vector potential. Since there are no source terms in Fourier regions, the magnetostatic Maxwell equation reduces to a Laplace equation. The resulting solution of the flux density can be written as,

$$\vec{B} = B_p \vec{p} + B_q \vec{q} = \sum_{n=1}^{\infty} \left(B_{psn} \sin(\omega_n q) + B_{pcn} \cos(\omega_n q) \right) \vec{p} + \sum_{n=1}^{\infty} \left(B_{qsn} \sin(\omega_n q) + B_{qcn} \cos(\omega_n q) \right) \vec{q}, \tag{1}$$

where B_{psn}, B_{pcn}, B_{qsn} and B_{qcn} are listed in TABLE III [6].

B. Definition of MEC regions

A MEC region is divided into elements with rectangular and circular sector shapes in Cartesian and polar coordinate systems, respectively. Each element contains the information of reluctance, permeability and magnetic source. An example of a meshed MEC region is shown in Fig. 3, as can be seen, the

TABLE IV
Distribution of current-related mmf in the Cartesian coordinate system.

Pos.	$\mathcal{F}^k_{p\pm}$ **for** J_1	$\mathcal{F}^k_{q\pm}$ **for** J_1	$\mathcal{F}^k_{p\pm}$ **for** J_2	$\mathcal{F}^k_{q\pm}$ **for** J_2
Yoke	0	$\mathcal{F}_{J1,q}$	0	$\mathcal{F}_{J2,q}$
Tooth	$\mathcal{F}_{J1,p}$	0	-$\mathcal{F}_{J2,p}$	0
Slot	$2x^k\mathcal{F}_{J1,p}/\tau_s$	$y^k\mathcal{F}_{J1,q}/h_t$	-$2x^k\mathcal{F}_{J2,p}/\tau_s$	$y^k\mathcal{F}_{J2,q}/h_t$

mesh is formed such that the material boundaries coincide with the mesh element edges, hence each MEC element contains homogeneous permeability [7]. In both $\pm p$- and $\pm q$-directions, a reluctance is assumed as shown in Fig. 3.

Magnetostatic problem in MEC regions is described using scalar potential. Each MEC element has a potential node, the flux goes into the node equals to the flux goes out, such conservation of flux gives [7],

$$\phi^k_{q-} + \phi^k_{p-} - \phi^k_{p+} - \phi^k_{q+} = 0. \tag{2}$$

The fluxes in (2) are defined by the potential of element k and its surroundings, e.g.,

$$\phi^k_{p-} = \frac{\psi^{k-L} - \psi^k + \mathcal{F}^{k-L}_{p+} + \mathcal{F}^k_{p-}}{\Re^{k-L}_{p+} + \Re^k_{p-}}, \tag{3}$$

where ψ^{k-L} represents the potential of element $k-L$ that is at the bottom of element k, while $\mathcal{F}^k_{p-}$, $\mathcal{F}^{k-L}_{p+}$, R^k_{p-} and R^{k-L}_{p+} represent the magnetomotive force (mmf) and reluctances in $p\pm$-directions for element k and $k-L$, respectively.

For elements that represent a PM, the definition of the mmf is determined by the magnetization and the element size

$$\mathcal{F}^k_{p+} = \mathcal{F}^k_{p-} = \vec{M}^k_p l^k_p \Big/ (2\mu^k_r) \tag{4}$$

$$\mathcal{F}^k_{q+} = \mathcal{F}^k_{q-} = \vec{M}^k_q l^k_q \Big/ (2\mu^k_r) \tag{5}$$

where $\vec{M}_p$, $\vec{M}_q$, l^k_p and l^k_q are the magnetization and dimensions of element k in the p-and q-directions. For elements related to current excitation, the distribution of the mmf sources has to fulfill the Ampere's law for any arbitrary paths. In [8], the current is expressed merely in the q-direction for the situation of homogeneous current density in one slot, while in this paper, mmf sources are modeled in both p- and q-directions for two current densities in one slot. The expressions of current related mmf are divided into three categories depending on the location, i.e. in the yoke, tooth or slot. The mmf in the yoke or tooth only has respectively the values in the q- or p-direction, while both terms are assumed in the slot. The magnitude of these mmf sources in the Cartesian coordinate system is illustrated in Fig. 4 and TABLE IV, that is basically linear to the x or y locations of the element (x^k or y^k) before reaching the coil edges. The derivation in the polar coordinate system is similar, and hence, not repeated here.

C. Boundary conditions

After obtaining the expressions of magnetic field inside the MEC and Fourier regions, the boundary conditions are defined. Between the Fourier and MEC regions, continuity of magnetic field has to be ensured. i.e., consistent normal flux density and tangential magnetic field intensity in both spatial frequency and space domains. The explanations are elaborated in [7]. At the edge of the outer air and shaft regions, the magnetic field vanishes to zero, the implementation is described in [7], [13].

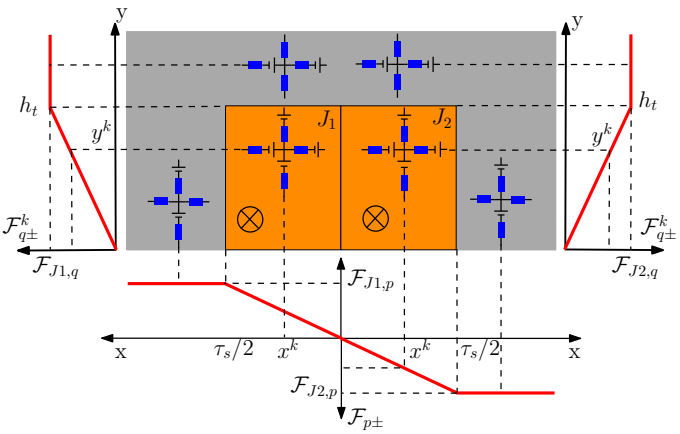

Fig. 4. Current related mmf for Cartesian coordinate system in the yoke, tooth and slot, where $\mathcal{F}_{J1,p} = J_1 A_s l^k_y/(4h_t)$, $\mathcal{F}_{J1,q} = J_1 A_s l^k_x/(2\tau_s)$, $\mathcal{F}_{J2,p} = J_2 A_s l^k_y/(4h_t)$, $\mathcal{F}_{J2,q} = J_2 A_s l^k_x/(2\tau_s)$ with $A_s = \tau_s h_t/2$.

III. Modeling of Nonlinear Material

The B-H characteristic of the soft magnetic material used in this paper is shown in Fig. 5. For a random working point C, the expression of B-H relationship can be locally linearized by a tangent line and the expression becomes,

$$H_C = \frac{B_C}{\mu_0 \Delta\mu_{r,iron}} - \frac{1}{\Delta\mu_{r,iron}} \frac{B_{r,iron}}{\mu_0} \tag{6}$$

where $\Delta\mu_{r,iron}$ is the incremental relative permeability defined by the slope of the tangent line and $B_{r,iron}$ is the remanent magnetic flux density defined by the intercept. By such expression, it is possible to make an analogy of the term '$B_{r,iron}/\mu_0$' to the magnetization of a PM. Since the magnitude of $B_{r,iron}$ is positively correlated to the flux density, the 'magnetization' is decomposed in $pq-$axes using the following expressions,

$$\vec{M}_{p,iron} = \frac{B_p}{\sqrt{B_p^2 + B_q^2}} \frac{B_{r,iron}}{\mu_0} \vec{p} \tag{7}$$

$$\vec{M}_{q,iron} = \frac{B_q}{\sqrt{B_p^2 + B_q^2}} \frac{B_{r,iron}}{\mu_0} \vec{q}, \tag{8}$$

which defines a Pythagorean theorem between flux density in pq-axes (B_q, B_q) and the 'magnetization'. As such, the material property of iron is defined by $\Delta\mu_{r,iron}$ and additional mmf sources obtained by (4)-(8).

The saturation problem is solved iteratively using the flowchart shown in Fig. 5. For each iterative step, the reluctances and mmf have to be re-calculated using the updated $\Delta\mu_{r,iron}$, $\vec{M}_{p,iron}$ and $\vec{M}_{q,iron}$. Values of B_p and B_q are derived by solving the boundary conditions with the newly defined MEC. Afterwards, $\Delta\mu_{r,iron}$, $\vec{M}_{p,iron}$ and $\vec{M}_{q,iron}$ are updated corresponding to the newly obtained B_p and B_q [14]. Different convergence conditions are applicable, e.g. difference of force or torque between two adjacent iterative steps is smaller than a certain level (0.2% in this paper).

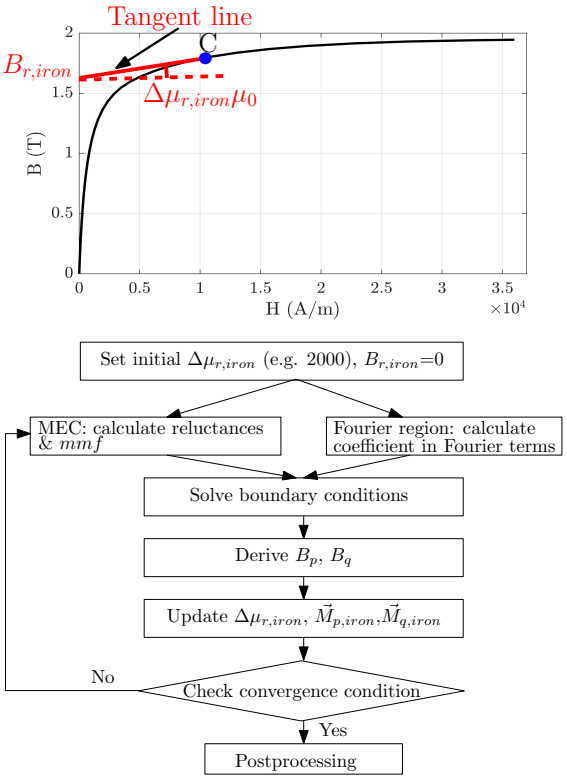

Fig. 5. *B-H* curve of the iron used in the examples and the flowchart of the HAM.

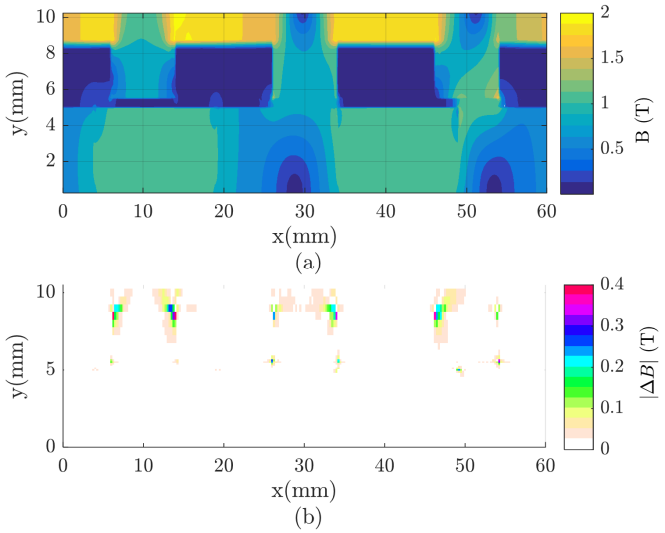

Fig. 6. Magnetic flux density for the PM machine: (a) the magnitude of flux density obtained by HAM and (b) the difference between FEA and HAM.

IV. FINITE-ELEMENT VERIFICATION

The modeling method is validated by FEA. For PM machine, the magnitude of the flux density obtained by HAM and the difference compared to FEA is shown in Fig. 6. For the SRM exmaple, the comparison of the flux density between HAM and FEA in the center of the airgap is shown in Fig. 7. The flux linkage waveforms for both machines is shown in Fig. 8. An overall excellent agreement is observed, showing that the algorithm for saturation is valid.

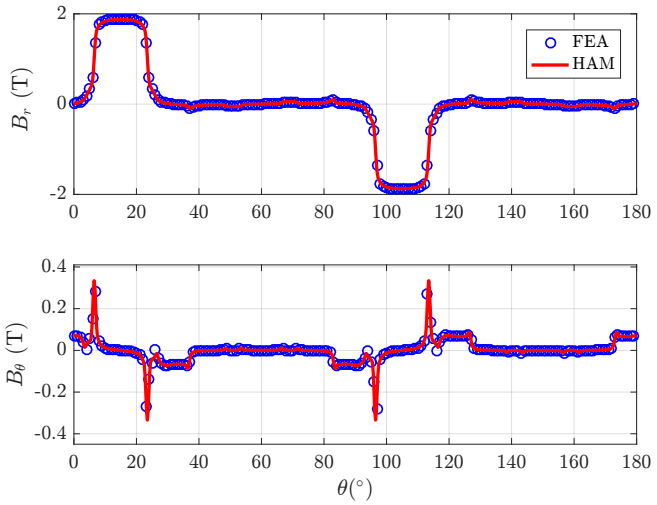

Fig. 7. Magnetic flux density obtained by FEA and HAM in the center of the airgap for the SRM (current density = 16 A/mm^2 in phase A): (a) radial and (b) circumferential component.

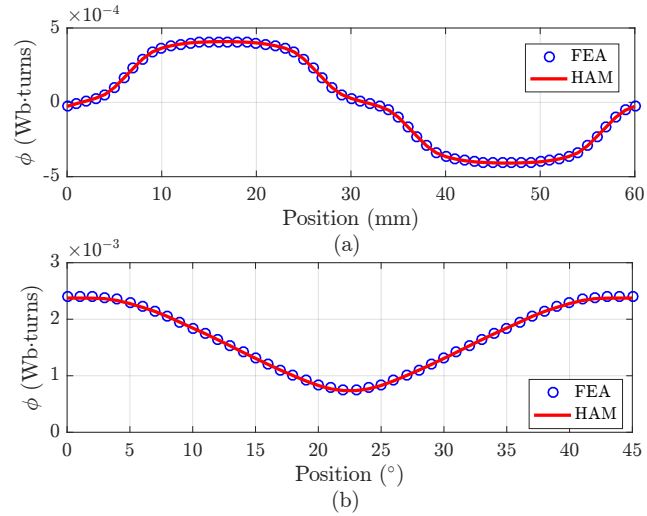

Fig. 8. Flux linkage waveforms of (a) phase A in PM machine at no load and (b) coil A_1 in SRM for current density = 16 A/mm^2 in phase A.

V. CONCLUSION

This paper uses the hybrid analytical modeling that integrates meshed MEC and Fourier modeling to calculate magnetic field in saturated electrical machines. It shows the capability to obtain accurate results in both Cartesian and polar coordinate systems with PM or current excitations. This method has the potential to be faster than FEA since the airgap region is not meshed, while a high mesh density is required in FEA. Additionally, since the expression of the magnetic field in the airgap is obtained analytically, force/torque calculations are straightforward and fast since the Maxwell stress tensor can be solved analytically. Furthermore, HAM implemented in Matlab can easily be integrated with algorithms for topology and geometry optimization. Future research will focus on implementation for different motor topologies, derivation of secondary parameters, etc.

REFERENCES

[1] R.L.J. Sprangers, J.J.H. Paulides, B.L.J. Gysen and E.A. Lomonova, *Magnetic saturation in semi-analytical harmonic modeling for electric machine analysis*, IEEE Trans. on Magn., vol. 52, no. 2, pp. 1-10, 2016.

[2] T. C. O'Connell and P. T. Krein, *The Schwarz-Christoffel analytical method applied to electric machine slot shape optimization*, IEEE Int. Elec. Mach. & Driv. Conf., pp. 341-346, 2007.

[3] D.C.J. Krop, *Integration of dual electromagnetic energy conversions: linear actuation with integrated contactless energy transfer*, Ph.D. dissertation, pp. 47-74, 2013.

[4] L. Gu, E. Bostanci, M. Moallem, S. Wang and P. Devendra, *Analytical calculation of the electromagnetic field in SRM using conformal mapping method*, 2016 IEEE Transp. Electr. Conf. and Expo. (ITEC), pp. 1-6, 2016.

[5] J. R. M. van Dam, J. J. H. Paulides, W. S. P. Robertson, M. Dhaens and E. A. Lomonova, *Analytical Surface Charge Method for Rotated Permanent Magnets: Boundary Element Method Comparison and Experimental Validation*, in IEEE Trans. on Magn,, vol. 52, no. 7, pp. 1-4, 2016.

[6] B.L.J. Gysen, K.J. Meessen, J.J.H. Paulides and E.A. Lomonova, *General formulation of the electromagnetic field distribution in machines and devices using Fourier analysis*, IEEE Trans. on Magn., vol. 46, no. 1, pp. 39-52, 2010.

[7] K.J.W. Pluk, J.W.Jansen and E.A. Lomonova, *Hybrid analytical modeling: Fourier modeling combined with mesh-based magnetic equivalent circuits*, IEEE Trans. on Magn., vol. 51, no. 8, pp. 1-10, 2015.

[8] S. Ouagued, Y. Amara and G. Barakat, *Comparison of hybrid analytical modelling and reluctance network modelling for pre-design purposes*, Mathematics and Computers in Simulation, Vol. 130, pp. 3-21, 2016.

[9] S. Ouagued, A. Aden Diriye, Y. Amara and G. Barakat, *A General Framework Based on a Hybrid Analytical Model for the Analysis and Design of Permanent Magnet Machines*, IEEE Transactions on Magnetics, Vol. 51, No. 11, pp. 1-4, 2015.

[10] S. Ouagued, Y. Amara and G. Barakat, *Cogging force analysis of linear permanent magnet machines using a hybrid analytical model*, IEEE Transactions on Magnetics, Vol. 52, No. 7, pp. 1-4, 2016.

[11] Y. Laoubi, M. Dhifli, G. Verez, Y. Amara, and G. Barakat, *Open circuit performance analysis of a permanent magnet linear machine using a new hybrid analytical model*, IEEE Trans. Magn., vol 51, no 3, pp. 14, 2015.

[12] W. Ding, L. Liu, J. Lou, and Y. Liu, *Comparative studies on mutually coupled dual-channel switched reluctance machines with different winding connections*, IEEE Trans. Magn., vol 49, no 11, pp. 5574-5589, 2013.

[13] B.L.J. Gysen, E. Ilhan, K.J. Messen, J.J.H. Paulides and E.A. Lomonova, *Modeling of flux switching permanent magnet machines with Fourier analysis*, IEEE Trans. on Magn., vol. 46, no. 6, pp. 1499-1502, 2010.

[14] A. Daghigh, H. Javadi and A. Javadi *Improved Analytical Modeling of Permanent Magnet Leakage Flux in Design of the Coreless Axial Flux Permanent Magnet Generatorx*, Canadian Journal of Elec. and Comput. Engineering, vol. 40, no. 1, pp. 3-11, 2017.